Design of Double Multilayer Monochromator for TXRF Optics by using Ray-Tracing Simulation

T.Yamada, A.Nisawa, T.Shoji and T.Utaka

X-ray Research Laboratory,Rigaku Corp.,Akaoji 14-8,Takatsuki,Osaka 569-1146,Japan

(Received October 12 1998; accepted January 11 1999)

A ray-tracing program was developed in order to design an intense and high-resolution monochromator for TXRF optics. A double multilayer monochromator was obtained as an optimized configuration for the incident beam of W-Lβ_1 line. Compared with a single multilayer monochromator it has an advantage that the intensity of W-Lα line is effectively diminished. Actual experiment showed that no peaks excited by the W-Lα line appeared in the spectrum of a blank Si wafer. The detection limit of Ni was improved if the double multilayer monochromator was used.

1. Introduction

TXRF(Total Reflection X-ray Fluorescence) is a powerful method to analyze trace elements on silicon wafers. It is essential for the TXRF instrument to have intense and high-resolution monochromator to achieve low detection limit in a range $10^9 \sim 10^{10}$ atoms/cm^2. Synthesized multilayer mirrors have high reflectivity for X-rays and are often used as the monochromators of TXRF instruments. The resolution of the multilayers, however, are not so high as that of LiF or Ge, which had been used as a monochromator. Poor resolution of the monochromator may cause often the appearance of ghost peaks in TXRF spectra. The W-Lα line(8.40keV) is one of the source of undesirable ghosts when the W-Lβ_1 line (9.67keV) is used to excite signals from constituents of the samples.

J.Knoth et al. pointed out that a double multilayer configuration is effective to decrease W-Lα line in the TXRF spectrum [1]. K.Stoev et al. optimized shapes of several multilayer mirrors for TXRF including double multilayer configurations by the study with ray-tracing and discussed the dependence of detection limits on the shape of the mirror [2]. As they mentioned, it is effective to use a double multilayer configuration for TXRF and is also effective to use ray-tracing technique to avoid complication in designing the optics.

It became necessary for us to design a new optics for the TXRF instrument detection limit of which should be 10^9 atoms/cm^2 for transition elements. We then developed a new ray-tracing program, which is suitable to simulate laboratory X-ray optics, and designed a double multilayer monochromator by optimizing several parameters of the configuration.

2.Ray-tracing

Ray-tracing simulation is a useful tool to design X-ray optics and has been often used for designing the optics of SR(Synchrotron Radiation) beam lines [3,4]. The simulation program, however, has not been used for laboratory optics so far. We developed a new ray-tracing simulation program suitable for laboratory X-ray optics and applied this to design TXRF optics. The program was made with NDP-FORTRAN-77 so as to run with a PC. The feature of the program is that the program trace X-ray path from the source to its terminal position one by one and calculated data are saved into a hard disk one by one. Large number up to several million of rays can be calculated this way. We can estimate the intensity of X-rays at an image plane fairly accurately by using a large number of rays.

Underwood et. al. gave formulae to calculate the reflectivity of X-rays from a multilayer [5]. We included these formulae into a subroutine in the program.

We simulated ray-tracing for two types of monochromators, the single multilayer configuration (SMC) and the double multilayer configuration (DMC). Figure 1 shows side views of the optics simulated. Fig.1A shows the trace for the SMC and Fig.1B for the DMC. X-ray source has an emission area of line focus, its effective area

being 10 x 0.05 mm^2. We gave the position and the direction of each X-ray on the source by a random creation. A multilayer mirror reflects X-rays with grazing angle of about 1 degree. Vertical axes of the figures are expanded to visualize the reflection. The tilting angle of the multilayer is adjusted so as to satisfy the Bragg condition for the W-Lβ_1 line. In these figures a thousand of traced rays are drawn so that the bunch of rays looks like black areas. Some of the X-rays go through the side of the multilayer and some are stopped by a slit situated above the multilayer. In Fig.1B, X-rays emitted from the X-ray source are reflected by the first multilayer then the second multilayer and finally arrive at an image plane. We can optimize the parameters of optics something like positions and tilting angles of the multilayers etc. by comparing these side views of ray-tracing. Figure 2 shows spot diagrams and intensity distribution of X-rays on the image planes. A hundred thousand of emitted rays were used in the calculation to draw these figures. The upper four figures show calculated results for SMC and the lower four for DMC. We performed the simulation for both the W-Lβ_1 line and the W-Lα line. The tilting angles of multilayers are adjusted to satisfy the Bragg condition for W-Lβ_1 lines. Thus the reflectivity of W-Lα lines are very weak. Density of the spot-diagram of W-Lα line is very low compared with that of W-Lβ_1 line. The horizontal axis of the intensity distribution of W-Lα line is expanded by a hundred times larger than that of W-Lβ_1 line. The intensity of W-Lα is estimated to be about 1/100 times of that of W-Lβ_1 in the case of SMC.

The intensity of the W-Lβ_1 line for DMC is about 0.7 times as that for SMC. The intensity of the W-Lα line for DMC is much weaker than that for SMC.

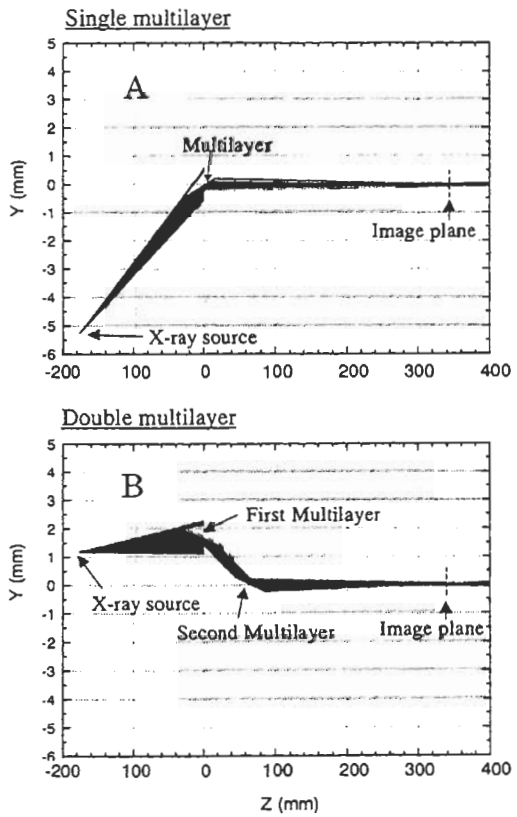

Figure 1. Side-views of ray-tracing simulation.

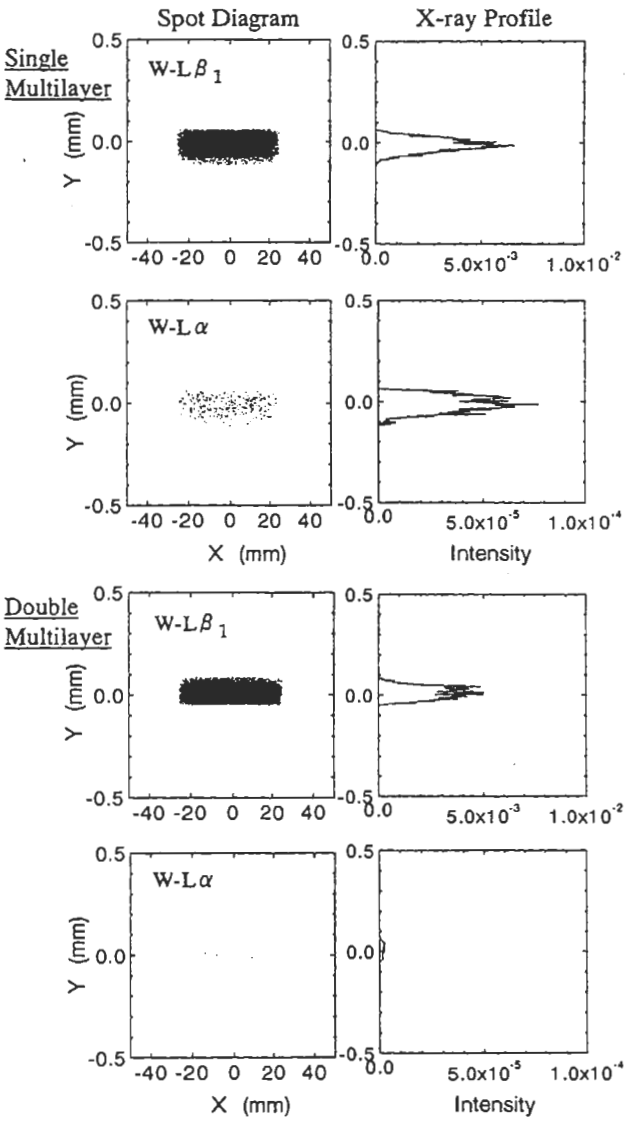

Figure 2. Spot diagram of X-rays on the image plane and intensity profile of X-rays in vertical direction.

Table 1. Comparison of Intensity of X-rays

Monochro -mator	Simulation			Experiment			
	W-Lβ$_1$ Intensity (arb.unit)	W-Lα Intensity (arb.unit)	W-Lα/ W-Lβ$_1$	Ni-Kα (cps/ 10^{10} atoms/cm^2)	background of Ni-Kα (cps)	Peak of W-Lα line	LLD (atoms/cm^2 for 1000sec)
Single multilayer	3.9	0.039	0.010	0.51	0.41	visible	0.14 x 10^{10}
Double multilayer	2.7	0.0019	0.00070	0.45	0.28	invisible	0.12 x 10^{10}

The left hand side of Table 1 shows numerical results of the intensity of X-rays calculated at the image plane for W-Lβ$_1$, W-Lα and their ratio W-Lα/W-Lβ$_1$. Intensity of W-Lβ$_1$ line for DMC is about 0.7 times of that of SMC. However the ratio W-Lα/W-Lβ$_1$ of DMC is about 14 times weaker than that of SMC. Therefore we expect that W-Lα can be effectively diminished from the TXRF spectrum by using DMC without a significant loss of intensity of incident X-rays.

3. Experiment

Figure 3 shows a schematic diagram of the TXRF instrument. This consists of an X-ray source, a monochromator, a specimen chamber and a detection system of X-rays. A rotating anode type X-ray source having a tungsten target operated with 30kV-300mA is installed. The X-rays of W-Lβ$_1$ line monochromatized by the monochromator impinge on the surface of a specimen with a grazing angle. Fluorescent X-rays from trace elements on the specimen are detected by a SSD and an energy dispersive spectrum is shown on a CRT. Figure 4 shows a typical example of the spectrum observed using a standard sample having transition elements of about 5 x 10^{14} atoms/cm^2. The peak of W-Lβ$_1$ is the reflection of the incident beams from the surface of the specimen and that of Si-Kα is the fluorescent X-rays from the substrate. Other peaks are the fluorescent X-rays emitted from the trace elements on the specimen surface. All the peaks of Fig.4 can be identified as shown in the figure and no ghost peaks are visible in this spectrum.

Some ghost peaks, however, are visible in spectra taken from blank samples if a single multilayer monochromator is utilized. Figure 5 shows their examples. Figs. A, B, and C are taken from the same position on a blank wafer with a monochromator of SMC. Glancing angles of the incident beam, ϕ, are the same but azimuth angles of the wafer, θ, are different as shown in the figures. Small peaks of W-Lα lines are visible in these figures and intensities of them change depending on the azimuth angle. These peaks are not due to the characteristic X-rays emitted from the elements on the specimen but to reflected X-rays

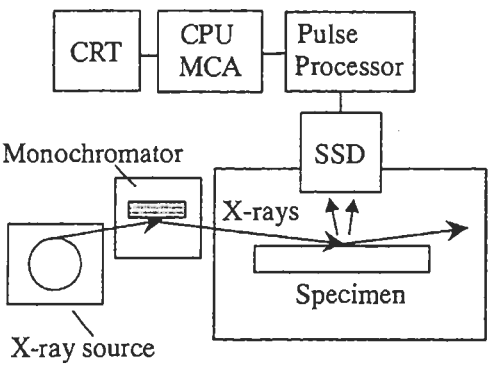

Figure 3. Schematic diagram of TXRF.

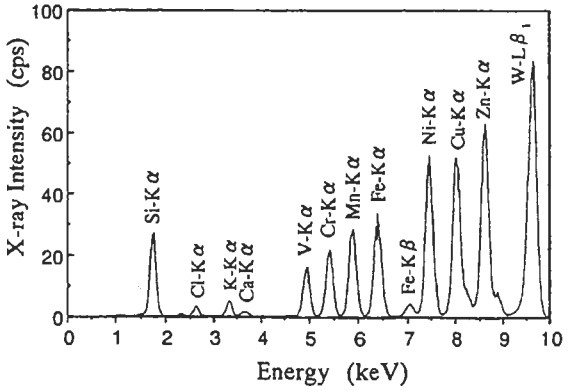

Figure 4. TXRF spectrum of a standard sample

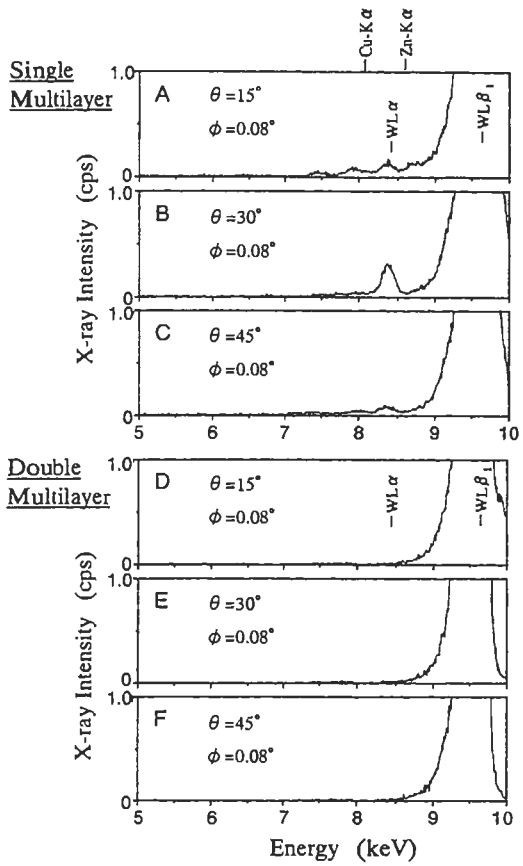

Figure 5. TXRF spectra of blank wafers, taken with a single multilayer monochromator(A,B,C), and with a double multilayer monochromator(D,E,F).

included in the incident beam. Azimuth dependence of the intensity is caused by the diffraction condition [6]. If the incident beam does not include any components of W-Lα lines such peaks do not appear in these spectra. The appearance of the peak of W-Lα line in the spectrum makes quantitative analysis of Cu and Zn inaccurate.

The actual optics based on the above calculation for DMC was made. Figs. D, E and F in Fig.3 are the results. As expected from the simulation, shown above, there are no visible peaks of the W-Lα line.

The performance of the TXRF instrument is characterized on the right hand side of Table 1. We compared the performance of SMC and DMC by the values of LLD(Lowest Limit of Detection) for Ni element as commonly treated. Intensity of Ni-Kα line was measured using a standard sample of 5 x 10^{12} atoms/cm^2 and the intensity of background was measured using a blank wafer. Glancing angle was ϕ= 0.08 degree. The intensity of the Ni-Kα line of DMC is about 0.8 times as that of SMC. The background of DMC is weaker than that of SMC. The resulting value of LLD of DMC is slightly improved owing to the decrease of the background.

4. Conclusion

From these results, we can conclude the following remarks. Ray-tracing simulation is effective to design the TXRF optics. Side-view figures of ray-tracing help us in optimizing the configuration. Amount of intensities of weak X-rays on the image plane can be estimated by a large number of emitted rays in the simulation. The experimental results proved the above conclusion from the simulation.

5.References

[1] J. Knoth, H. Schneider and H. Schwenke, X-ray Spectorometry, **23**, 261 (1994).
[2] K. Stoev, J. Knoth and H. Schwenke, X-ray Spectorometry, **27**, 166 (1998).
[3] B. Lai and F. Cerrina, Nucl. Instrum. & Methods, A**246**, 337 (1986).
[4] Y. Muramatsu, Y. Ohishi and H. Maezawa, Jpn. J. Appl. Phys., **27**, L1539 (1988).
[5] J. H. Underwood et al, "Low Energy X-ray Diagnostics-1981", p.170 (1981).
[6] T. Yamada and T. Arai, Advances in X-Ray Chemical Analysis, JAPAN, **26s**, 29(1995).